



Kinetics of the tungsten hexafluoride-silane reaction for the chemical vapor deposition of tungsten by Huseyin Gokce

A thesis submitted in partial fulfillment of the requirements for the degree of Doctor of Philosophy in Chemical Engineering

Montana State University

© Copyright by Huseyin Gokce (1991)

Abstract:

Tungsten has been used for multilevel metallization in very large scale integration (VLSI) technology. Reduction by silane has been considered as a high-rate, low-temperature process alternative to hydrogen reduction of tungsten hexafluoride in the chemical vapor deposition of W. In the present study, the kinetics of the low pressure chemical vapor deposition (LPCVD) of tungsten by silane reduction of tungsten hexafluoride on Si(100) surfaces was studied.

A single-wafer, cold-wall reactor was used for the experiments. The SiH<sub>4</sub>/WF<sub>6</sub> ratio was 1.0. The pressure and temperature range were 1-10 torr and 137-385°C, respectively. Kinetic data were obtained in the absence of mass transfer effects. The film thicknesses were measured by gravimetry. Scanning electron microscopy (SEM), Auger electron spectroscopy (AES), x-ray diffraction (XRD), and resistivity measurements were used to analyze the W films.

For the horizontal substrate position and 4-minute reaction times, the apparent activation energies were determined to be 0.35 eV/atom for 10 torr, 0.17 eV/atom for 3 torr, and 0.08 eV/atom for 1 torr. Lower temperatures and higher pressures produced porous films, while higher temperatures and lower pressures resulted in continuous films with smoother surfaces. At the Si-W interface, a W(110) preferential orientation was observed. As the W films grew thicker, W orientation switched from (110) to (100). Apparent activation energy seems to change with thickness.

Si and F contents of the films were within the noise level for Auger detection. Porosity was found to be influential in the film resistivity.

The higher activation energy observed at higher pressure was deduced to be a result of limitations in the rate of SiH<sub>4</sub> adsorption and subsequent adatom surface diffusion. The domination of W(100) orientation for thick films at high temperatures was attributed to a reconstruction of W(100) surfaces on which adatom surface diffusion is easier.

KINETICS OF THE TUNGSTEN HEXAFLUORIDE-SILANE REACTION  
FOR THE CHEMICAL VAPOR DEPOSITION OF TUNGSTEN

by  
Huseyin Gokce

A thesis submitted in partial fulfillment  
of the requirements for the degree

of  
Doctor of Philosophy  
in  
Chemical Engineering

MONTANA STATE UNIVERSITY  
Bozeman, Montana

June 1991

D378  
G5615

ii

APPROVAL

of a thesis submitted by

Huseyin Gokce

This thesis has been read by each member of the thesis committee and has been found to be satisfactory regarding content, English usage, format, citations, bibliographic style, and consistency, and is ready for submission to the College of Graduate Studies.

July 29, 1991  
Date

John T. Sears  
Chairperson, Graduate Committee

Approved for the Major Department

July 29, 1991  
Date

John T. Sears  
Head, Major Department

Approved for the College of Graduate Studies

August 6, 1991  
Date

Henry L. Parsons  
Graduate Dean

## STATEMENT OF PERMISSION TO USE

In presenting this thesis in partial fulfillment of the requirements for a doctoral degree at Montana State University, I agree that the Library shall make it available to borrowers under rules of the Library. I further agree that copying of this thesis is allowable only for scholarly purposes, consistent with "fair use" as prescribed in the U.S. Copyright Law. Requests for extensive copying or reproduction of this thesis should be referred to University Microfilms International, 300 North Zeeb Road, Ann Arbor, Michigan 48106, to whom I have granted "the exclusive right to reproduce and distribute copies of the dissertation in and from microfilm and distribute by abstract in any format."

Signature Date July 29, 1991

Dedicated to my parents,  
Habibe and Emin Gokce

**ACKNOWLEDGEMENTS**

I wish to express my deepest gratitude to Dr. John T. Sears for his guidance and encouragement throughout the course of this research. Likewise, I am indebted to Dr. Turgut Sahin for his continuous support and technical advice even after assuming a position in industry.

I wish to express my special thanks to Dr. Max C. Deibert and Dr. John F. Mandell of Chemical Engineering Department and Dr. Recep Avci of Physics Department at MSU for their helpful suggestions during this study.

My fellow graduate students and the staff of the Chemical Engineering Department have created a very pleasant working environment, I gratefully acknowledge their help and friendship. Lyman Fellows deserves special appreciation for his help in the maintenance of the equipment.

My thanks are due to Dr. William Inskip of Plant and Soil Science at MSU for his help with the x-ray diffraction facility. This research would not have occurred without the silicon wafers supplied by Dr. Robert S. Blewer of Sandia National Laboratories, his help is gratefully acknowledged.

Financial support provided in part by Montana Science and Technology Alliance is acknowledged.

Last, but not the least, I would like to take this opportunity to thank my parents for their unending moral support, understanding and patience throughout this work.

## TABLE OF CONTENTS

	Page
LIST OF TABLES.....	ix
LIST OF FIGURES.....	x
ABSTRACT.....	xiv
1. INTRODUCTION.....	1
Research Objective.....	3
2. LITERATURE SURVEY.....	5
Thin Films.....	5
Thin Film Formation.....	6
Condensation and Nucleation.....	7
Film Growth.....	13
The Island Stage.....	14
The Coalescence Stage.....	14
The Channel Stage.....	16
The Continuous Film.....	16
Growth Modes.....	17
Epitaxial Growth.....	19
Thin Film Analysis Techniques.....	20
X-ray Diffraction.....	20
Diffractometer Method.....	22
Sheet Resistance.....	23
Four-point Probe Method.....	23
Scanning Electron Microscopy.....	26
Auger Electron Spectroscopy.....	29
Film Thickness Measurement.....	34
Chemical Vapor Deposition.....	37
Basic Steps in CVD.....	38
Experimental Parameters in CVD.....	39
Deposition Temperature.....	39
Gas Flow Rate.....	44
Crystallographic Orientation.....	47
Substrate Position.....	48
Reactant Partial Pressure.....	49
Surface Area.....	49
Chemical Vapor Deposition Reactors.....	49
Hot-wall Reactors.....	50
Cold-wall Reactors.....	50
Atmospheric Pressure Reactors.....	50
Low-pressure CVD Reactors.....	52
Plasma-enhanced CVD Reactors.....	54
Photon-induced CVD Reactors.....	55
Chemical Vapor Deposition of Tungsten.....	56
Reactions for CVD of Tungsten.....	59
Si Reduction of $WF_6$ .....	61

## TABLE OF CONTENTS (Continued)

	Page
H <sub>2</sub> Reduction of WF <sub>6</sub> .....	66
SiH <sub>4</sub> Reduction of WF <sub>6</sub> .....	71
3. EXPERIMENTAL.....	85
Reaction System.....	84
Equipment.....	84
Gas Lines and Controllers.....	84
Reactor.....	86
Pressure Controller.....	89
Pumps.....	89
Effluent Gas Treatment.....	90
Oil Filtering System.....	91
Experimental Procedure.....	92
Sample Preparation.....	92
Deposition.....	92
Reactor Preparation.....	92
Reactor Operation.....	94
Data Analysis.....	94
Sheet Resistance Measurement.....	95
Film Thickness Measurement.....	95
SEM Analysis.....	96
AES Analysis.....	97
X-ray Diffraction Analysis.....	98
Scope of the Experiments.....	98
4. RESULTS.....	101
Preliminary Experiments.....	101
AES Analysis.....	104
Kinetics-Gravimetric.....	109
SEM Analysis.....	111
Time-dependent Experiments.....	111
Overgrown Films.....	119
4-Minute Experiments.....	121
X-ray Diffraction Analysis.....	128
Film Resistivity.....	133
5. DISCUSSION.....	138
Verification of Kinetic W Deposition.....	138
Impurity Content.....	138
Kinetic Region Gas Flow Rate.....	142
Effect of Substrate Position on Kinetics.....	145
Kinetics and Morphology.....	146
Morphology, Nucleation and Growth.....	146
Crystal Structure.....	151
Tungsten Growth on Si.....	152

## TABLE OF CONTENTS (Continued)

	Page
Tungsten Growth on W.....	155
Crystallinity and Crystal Size.....	159
Proposed Kinetic Steps.....	163
Film Properties.....	173
Film Resistivity.....	173
Adhesion and Stress.....	175
6. SUMMARY AND CONCLUSIONS .....	178
7. RECOMMENDATIONS.....	182
REFERENCES CITED.....	186
APPENDICES.....	196
APPENDIX A-Potential Hazards of the Reaction Gases.....	197
Abbreviations.....	198
Hydrogen Fluoride (HF).....	198
Tungsten Hexafluoride (WF <sub>6</sub> ).....	199
Silicon Tetrafluoride (SiF <sub>4</sub> ).....	199
Hydrogen (H <sub>2</sub> ).....	199
Silane (SiH <sub>4</sub> ).....	199
Safety in the Reactor System.....	200
APPENDIX B-Calculation of Reactant Fractional Conversion.....	201
APPENDIX C-Prediction of Transport Properties for Reaction Gases.....	204
APPENDIX D-Reynolds Number Calculation.....	207
APPENDIX E-Sample Calculation for Mass Flux to the Substrate.....	212
APPENDIX F-X-ray Diffraction Line Data for Tungsten Phases.....	219
APPENDIX G-Tungsten Crystal Size Calculation.....	222
The Scherrer Formula.....	223
Sample Calculation for W Crystal Size.....	223
APPENDIX H-SEM Micrographs for Time-dependent Experiments.....	225

## LIST OF TABLES

Table	Page
1. Free Energy Change at 600 K.....	60
2. Tungsten Phases and Their Properties.....	81
3. Specification of the Reaction Gases.....	86
4. AES Sensitivity Factors.....	97
5. Gas Flow Conditions.....	100
6. X-ray Diffraction Intensities of Tungsten Films.....	131
7. X-ray Diffraction Peak Widths of Tungsten Films.....	132
8. Lattice Mismatch, $\epsilon$ , Between Si and W Crystal Surfaces.....	153
9. Calculated Grain Sizes and Measured Aggragate Sizes for Tungsten Films.....	161
10. Tungsten Deposition Rates at 285°C, Experimental versus Theoretical at $X_{\text{SiH}_4} = 1.0$ .....	167
11. Slopes for Sheet Resistance versus Inverse Deposition Time.....	175
12. Critical Properties for the Reactant Gases.....	205
13. Lennard Jones Parameters for the Reactant Gases.....	206
14. Transport Properties for the Reactant Gases at 285°C.....	206
15. Gas Phase Composition of the Reactant Gases.....	208
16. X-ray Diffraction Lines for $\alpha$ -W.....	220
17. X-ray Diffraction Lines for $\beta$ -W.....	221
18. X-ray Diffraction Lines for $\text{W}_3\text{Si}_5$ .....	221

## LIST OF FIGURES

Figure	Page
1. Saturation density of nuclei vs. reciprocal temperature.....	12
2. (a) Schematic of the stages of film growth.....	15
(b) Schematic of the shape changes during coalescence.....	15
3. Various modes of growth of an overlayer on a substrate.....	18
4. Equivalence of a second order reflection.....	21
5. X-ray diffractometer configuration.....	21
6. Definition of sheet resistance.....	24
7. Schematic diagram for a four-point probe measuring setup.....	24
8. Positive and negative sources relative to point P.....	24
9. (a) Energy spectrum of electrons emitted from a surface bombarded by an electron beam.	
(b) The derivative of the number of emitted electrons with respect to the energy.....	27
10. Schematic drawing of a scanning electron microscope....	27
11. X-ray and Auger electron emission during de-excitation of atom after initial ionization.....	30
12. Auger spectrum of W film surface on Si.....	33
13. Temperature dependence of growth rate for CVD films....	42
14. Reaction rate as a function of reciprocal temperature for zero and negative heat of reaction.....	43
15. Reaction rate as a function of reciprocal temperature for positive heat of reaction.....	45
16. Idealized growth-rate versus fluid flow-rate plot showing the different growth regimes.....	46
17. Schematic diagrams of CVD reactors.....	51
18. Address access time as a function of gate length.....	57

## LIST OF FIGURES (Continued)

Figure	Page
19. Future applications of refractory metals and/or metal silicides.....	59
20. Schematic illustration of several problems associated with selective W deposition by LPCVD.....	62
21. Arrhenius plot of deposition rate of CVD tungsten by H <sub>2</sub> reduction of WF <sub>6</sub> .....	68
22. Normalized x-ray texture as a function of film thickness.....	72
23. Arrhenius plot for SiH <sub>4</sub> -WF <sub>6</sub> reaction system [7].....	74
24. Arrhenius plot of H <sub>2</sub> and SiH <sub>2n+2</sub> (n = 1-3) reduction of WF <sub>6</sub> [8].....	74
25. Arrhenius plot for SiH <sub>4</sub> /WF <sub>6</sub> < 0.9 [9].....	76
26. Arrhenius plot of blanket W deposition [10].....	76
27. Schematic diagram of the LPCVD reaction system.....	85
28. Cross-sectional view of the LPCVD reactor.....	88
29. Preliminary experiments to assure differential reactor.....	103
30. Auger depth profile for W film deposited at 10 torr and 137°C.....	105
31. Auger depth profile for W film deposited at 1 torr and 137°C.....	106
32. Auger depth profile for W film deposited at 3 torr and 385°C.....	107
33. Arrhenius plot for WF <sub>6</sub> -SiH <sub>4</sub> system. Substrate horizontal.....	110
34. Arrhenius plot for WF <sub>6</sub> -SiH <sub>4</sub> system. Substrate vertical.....	112
35. SEM micrographs of W surfaces at different reaction times.....	114

## LIST OF FIGURES (Continued)

Figure	Page
36. SEM micrographs of W surfaces, t = 1.5 min, P = 10 torr.....	115
37. SEM micrographs of W surfaces, t = 1.5 min, P = 1 torr.....	116
38. Aggregate growth rate, parallel to surface, P = 10 torr.....	117
39. Aggregate growth rate, parallel to surface, P = 1 torr.....	118
40. Arrhenius plot for W aggregate growth.....	120
41. SEM micrographs of tungsten surfaces, t = 12 min.....	122
42. SEM micrographs of tungsten surfaces, t = 10 min.....	123
43. SEM cross-sectional view of tungsten film, t = 12 min.....	124
44. SEM cross-sectional views of tungsten films, t = 10 min.....	125
45. SEM surface micrographs of W deposited at 385°C.....	126
46. SEM surface micrographs of W deposited at 137°C.....	127
47. X-ray diffraction patterns of W films deposited at T = 285°C and P = 1 torr.....	130
48. Resistivity versus W film thickness.....	134
49. Sheet resistance versus inverse deposition time for P = 10 torr.....	136
50. Sheet resistance versus inverse deposition time for P = 1 torr.....	137
51. Schematic diagrams of W(100) surfaces.....	158
52. The mosaic structure of a real crystal.....	162
53. Arrhenius plots for adsorption of silane on Si(111)-(7x7).....	169
54. SEM micrographs of W surfaces deposited at different reaction times, P = 10 torr, T = 285°C.....	226

## LIST OF FIGURES (Continued)

Figure	Page
55. SEM micrographs of W surfaces deposited at different reaction times, P = 10 torr, T = 330°C.....	227
56. SEM micrographs of W surfaces deposited at different reaction times, P = 10 torr, T = 385°C.....	228
57. SEM micrographs of W surfaces deposited at different reaction times, P = 1 torr, T = 285°C.....	229
58. SEM micrographs of W surfaces deposited at different reaction times, P = 1 torr, T = 330°C.....	230
59. SEM micrographs of W surfaces deposited at different reaction times, P = 1 torr, T = 385°C.....	231

## ABSTRACT

Tungsten has been used for multilevel metallization in very large scale integration (VLSI) technology. Reduction by silane has been considered as a high-rate, low-temperature process alternative to hydrogen reduction of tungsten hexafluoride in the chemical vapor deposition of W. In the present study, the kinetics of the low pressure chemical vapor deposition (LPCVD) of tungsten by silane reduction of tungsten hexafluoride on Si(100) surfaces was studied.

A single-wafer, cold-wall reactor was used for the experiments. The  $\text{SiH}_4/\text{WF}_6$  ratio was 1.0. The pressure and temperature range were 1-10 torr and 137-385°C, respectively. Kinetic data were obtained in the absence of mass transfer effects. The film thicknesses were measured by gravimetry. Scanning electron microscopy (SEM), Auger electron spectroscopy (AES), x-ray diffraction (XRD), and resistivity measurements were used to analyze the W films.

For the horizontal substrate position and 4-minute reaction times, the apparent activation energies were determined to be 0.35 eV/atom for 10 torr, 0.17 eV/atom for 3 torr, and 0.08 eV/atom for 1 torr. Lower temperatures and higher pressures produced porous films, while higher temperatures and lower pressures resulted in continuous films with smoother surfaces. At the Si-W interface, a W(110) preferential orientation was observed. As the W films grew thicker, W orientation switched from (110) to (100). Apparent activation energy seems to change with thickness.

Si and F contents of the films were within the noise level for Auger detection. Porosity was found to be influential in the film resistivity.

The higher activation energy observed at higher pressure was deduced to be a result of limitations in the rate of  $\text{SiH}_4$  adsorption and subsequent adatom surface diffusion. The domination of W(100) orientation for thick films at high temperatures was attributed to a reconstruction of W(100) surfaces on which adatom surface diffusion is easier.

## CHAPTER 1

## INTRODUCTION

In the mid 1970's, very large scale integration (VLSI) technology started with 64Kbit dynamic random access memory for dynamic memory devices and specific integrated circuits. The technology has recently improved to provide 16Mbit capacities. It is predicted that at the end of the 20th century, dynamic memory chips will reach 1 gigabit capacity [1]. This much memory is only one-tenth of the number of neurons in a human brain. Thus, one memory board would be equivalent to a human brain in terms of data storage.

The developments in the VLSI technology have been making ultra-large scale integration (ULSI) technology a coming reality, as submicron dimensions can be utilized. Such a transmutation in the technology has certain requirements. Some of them include high aspect via-contacts, complicated geometry in multi-level interconnections, high current density, and shallow junctions at source/drain regions. These requirements have directed the researchers to look for new materials which can provide low contact resistance, smooth interconnections to prevent electromigration, and low temperature processibility.

It has been shown that selectively deposited tungsten (1,000 - 1,500 Å) on monosilicon or polysilicon surfaces in metal-oxide silicon (MOS) device structures can serve as an

interconnect shunt and contact diffusion barrier [2]. The term "selective deposition" is used when tungsten (W) is deposited only onto silicon (Si) and surrounding silicon dioxide ( $\text{SiO}_2$ ) is free of deposition.

Tungsten hexafluoride, a commonly used source gas for tungsten deposition, can be reduced by either silane, hydrogen or silicon substrate itself. The kinetics for tungsten deposition by Si and  $\text{H}_2$  reduction of  $\text{WF}_6$  has been studied extensively and the parameters have been well established [3-6]. The Si reduction reaction causes the consumption of the silicon substrate and produces very rough W-Si interfaces. The deposition reaction stops after a limiting W film thickness is reached (~300 - 400 Å).  $\text{H}_2$  reduction reaction does not show a self-limiting behavior but has some drawbacks, such as silicon consumption of the substrate which appears in the form of tunnels and required high deposition temperatures for practical deposition rates.

Chemical vapor deposition (CVD) of tungsten by hydrogen ( $\text{H}_2$ ) reduction of tungsten hexafluoride ( $\text{WF}_6$ ) is considered to be a potential technique for integrated-circuit applications. Low pressure chemical vapor deposition (LPCVD) has some proven advantages over atmospheric pressure CVD. These advantages are increased control over the deposition ambient, greater throughput, lower reactant gas flows, high purity deposits, and excellent deposit uniformities and conformities.

Silane ( $\text{SiH}_4$ ) reduction of  $\text{WF}_6$  was shown to suppress silicon consumption and tunneling [7,8]. Therefore, the leakage current and contact resistance is low, which are the desired electrical properties. Kinetic studies on the LPCVD of tungsten using  $\text{SiH}_4$ - $\text{WF}_6$  reaction system have been very limited since most studies aimed at developing a better tungsten film quality rather than establishing the kinetic parameters [7-10]. All the researchers have observed a complicated behavior in the temperature dependence of the kinetics of the  $\text{SiH}_4$ - $\text{WF}_6$  reaction, and thus, no Arrhenius activation energies have been reported.

#### Research Objective

An efficient design for a commercial production system requires knowledge of reaction kinetic parameters. The lack of kinetic parameters for the  $\text{SiH}_4$ - $\text{WF}_6$  system is the motivation for this study. The research objectives are:

- (1) To measure and evaluate kinetic data for the chemical vapor deposition of tungsten by  $\text{SiH}_4$  reduction of  $\text{WF}_6$ . The substrate surface is to be Si(100) and the kinetic data will be acquired under differential reactor conditions. The deposition rates will be determined by a gravimetric method.
- (2) To examine the quality of the tungsten films deposited by the  $\text{WF}_6$ - $\text{SiH}_4$  reaction. Thin W films will be analyzed with

scanning electron microscopy (SEM), x-ray diffraction (XRD), Auger electron spectroscopy (AES), and resistivity measurements.

- (3) To interpret the kinetic data in the context of the morphology and crystal structure studies. Parameters are the reaction temperature and pressure, the gas flow rate, the film morphology, and the crystal orientation.

## CHAPTER 2

## LITERATURE SURVEY

Thin Films

VLSI devices use a variety of thin films as metals, semiconductors, and insulators. A better understanding of chemical and physical properties of thin films is essential to improve the device performance. There are specific methods developed to form thin films for different applications [11]. Regardless of the method of formation, VLSI fabrication requires that the process be economical and the resultant film have the following properties [12]:

- Good thickness uniformity.
- High purity and high density to provide good insulation (or conduction) and integrity.
- Controlled composition and stoichiometries.
- High degree of structural perfection to ensure film continuity over the lifetime of the device.
- Good electrical properties.
- Excellent adhesion and low stress values to eschew film discontinuity due to deformation, cracking, undercutting, and lifting effects.
- Good step coverage.

It is known that the properties of a thin film may be quite different from those of the bulk material. These differences are more pronounced as the film thickness gets extremely small, namely at the micron level. For one thing, thin films have a higher surface-to-volume ratio than a bulk material which makes the surface properties more influential on the film properties. For another, the peculiar structure of the thin film is an important factor in determining the film properties, and this structure is dictated by the nature of the processes which occur during film formation.

### Thin Film Formation

Thin films can be formed by a large variety of techniques [13]. In VLSI fabrication, the formation of thin films can be categorized into two major procedures:

- (1) Film growth by interaction of a vapor-deposited species with the substrate.
- (2) Film formation without causing changes to the substrate.

The first category includes thermal oxidation and nitridation of single crystal silicon and polysilicon substrates, and the formation of silicides by direct reaction of a predeposited metal and the substrate.

The second category includes three forms of deposition on the substrate:

i) Chemical vapor deposition (CVD), where solid films are deposited on a substrate by reacting vapor phase chemicals on the substrate surface. Amorphous, polycrystalline and single-crystalline films can be formed by CVD. The process is called epitaxy when CVD is used to form single-crystal thin films.

ii) Physical vapor deposition (PVD), where the atoms of the material to be deposited are physically dislodged from a source material into vacuum, then the condensation occurs on the substrate to form the thin film. PVD processes include evaporation, sputtering and molecular beam epitaxy.

iii) The deposition of a liquid on a substrate which is then dried to form the solid thin film. Spin-coating is the most commonly used technique.

Thin film deposition by most common processes, such as PVD and CVD, involves a condensation transformation from the vapor to the solid phase. The formation of a thin film can be best understood by the thermodynamic and kinetic analysis of the condensation phenomena [14,15].

### Condensation and Nucleation

The initial step of thin film nucleation in CVD and PVD is the impingement of vapor molecules onto the substrate. After impingement, the vapor molecules can either adsorb and stick permanently to the substrate, or they adsorb momentarily and re-evaporate, or they ricochet back to the vapor phase.

The initial attraction of the impinging atom (or molecule) requires that instantaneous dipole or quadrupole moments of the surface atoms exist. The excess energy of the attracted atom is transferred to the substrate in the form of lattice oscillations. The attracted atom then becomes attached to the surface after losing its velocity component normal to the surface. The attachment of impinging vapor atoms on the surface is known as "adsorption" and the adsorbed atom is called "adatom".

Two types of adsorption phenomena have been recognized in principle:

i) Physisorption caused by secondary (van der Waals) attractive forces.

ii) Chemisorption caused by chemical bonding involving transfer of electrons between adsorbent and adsorbate.

Because of the nature of the bonding involved, physisorption is associated with much smaller binding energies ( $\sim 0.25$  eV) than is chemisorption (8-10 eV).

Adsorbent surfaces may be pictured as an array of adsorption sites where each adsorbed molecule occupies a minimum potential energy site [16]. An adsorbed atom may retain its initial lateral momentum or may be activated thermally from the surface so that it will jump over the energy barriers into the next available adsorption site. It is also possible that some of the adatoms re-evaporate from the surface into the vapor phase. The factors that affect the

rates of adsorption and desorption (re-evaporation) are given by the functions below, in which the variables are assumed separable. Then rate of adsorption,  $\mu_a$ , is [17]

$$\mu_a = \frac{P}{\sqrt{2\pi mkT}} \sum_{i=1}^m n_i \sigma_i f(\theta_i) e^{-E_i/RT} \quad (1)$$

and rate of desorption,  $\mu_d$ , is

$$\mu_d = \sum_{i=1}^m n_i K_i f'(\theta_i) e^{-E'_i/RT} \quad (2)$$

where,

$m$  : number of types of sites.

$n_i$  : number of sites of type (i).

$\theta$  : surface coverage.

$f(\theta)$ ,  $f'(\theta)$  : function for the surface coverage dependence of adsorption and desorption, respectively.

$R$  : gas constant.

$E$ ,  $E'$  : activation energy of adsorption and desorption, respectively.

$\sigma$ ,  $K$  : condensation and evaporation probability, respectively.

$P/(2\pi mkT)^{0.5}$  : number of collisions with a surface

( $m$  : mass of atom,  $k$  : Boltzmann constant).

Equations 1 and 2 indicate that adsorption rate is a function of both pressure,  $P$ , and temperature,  $T$ , while desorption rate is not influenced by pressure, but by temperature.

As the adatoms migrate along the surface, they collide with other atoms and form clusters of adsorbed atoms. The

small clusters consist of only a few atoms and have very high surface-to-volume ratios. This results in high surface energy values and energetically unstable clusters which have a high tendency to re-evaporate. For this reason, most theories on condensation and nucleation define a critical radius for clusters above which the total free energy of the system decreases with increasing radius. Hence, clusters larger than this critical size are stable and favor a continued growth. The stable clusters are called "nuclei" and the mechanism of their formation is termed "nucleation".

There are two basic models to explain the nucleation phenomena: the capillarity model which employs simple idealized geometrical shapes for the cluster [18,19], and the atomistic (or statistical) model [20] which uses only discrete arrangements of atoms. Furthermore, the capillarity model predicts a continuous variation of crystal size and nucleation rate with the degree of supersaturation, whereas the atomistic model predicts discontinuous changes which are more pronounced for smaller critical cluster sizes. In the limit of large critical nuclei, the two models become identical.

In the initial stages of condensation, clusters of various sizes are in metastable equilibrium with free adatoms. As the clusters grow to supercritical dimensions, they deplete the adatoms within their surrounding regions in which any further cluster formation (or nucleation) is not possible. These regions are called "capture zones".

It is observed that the film mass deposited depends on the total impingement time, the substrate temperature, the diffusion coefficient of adatoms on the surface, the mean residence time of adatoms, and the impingement rate [21]. The "onset" of condensation is defined by the initial formation of nuclei and is marked experimentally by the appearance of some observable mass of condensate on the substrate. The corresponding substrate temperature is called the "critical" condensation temperature. The critical temperature,  $T_c$ , however, depends on the observation time. If the adatoms have long enough mean free residence times of adherence on the surface at temperature  $T_c$ , all impinged atoms will be captured by stable nuclei so that the sticking coefficient will be unity even initially. For temperatures greater than  $T_c$ , the adatoms have less residence time on the surface due to increased desorption from the surface, therefore longer times are required for the onset of condensation.

Lewis and Campbell [22] have analyzed the nucleation process near  $T_0$  for the case of the smallest possible critical nucleus. Figure 1 shows how the saturation density of nuclei changes with temperature and identifies incomplete and complete condensation temperature regions. At low temperatures or high impingement rates (complete condensation), the

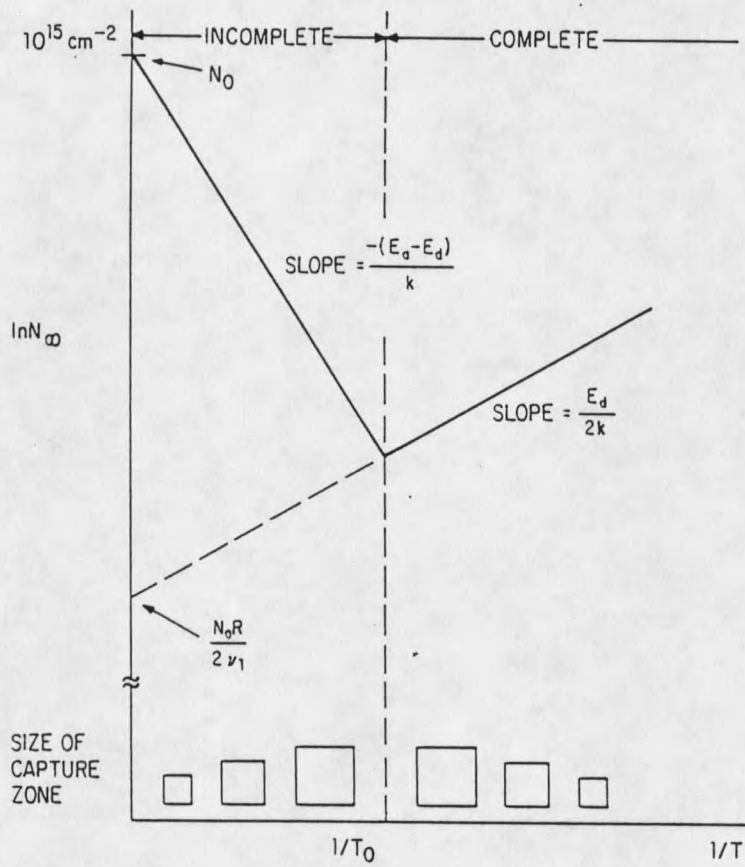


Figure 1. Saturation density of nuclei vs. reciprocal temperature, illustrating the boundary between initially complete and incomplete condensation [22].

impinged atoms immediately form stable pairs of density  $N_0$  without the possibility of re-evaporation. In this region, the slope of the  $\ln N_0$  vs.  $1/T$  plot is positive since the diffusion coefficient increases with increasing temperature, hence increasing the size of the capture zone where further nucleation is not possible. At high temperatures (incomplete condensation), the slope is negative because increased temperatures lead to re-evaporation of adatoms which means smaller mean residence times. The result is decreased size of the capture zone around each nucleus, yielding more nuclei on the substrate.

Zinsmeister [23] has claimed that the desorption and evaporation of clusters, as well as adatoms, are not negligible in spite of the much greater activation energy involved. He indicated that at the beginning of the condensation, adatoms and very small clusters predominate, but later most of the condensate is tied up in larger clusters. He also showed that the sticking coefficient is low at the beginning of the condensation.

### Film Growth

Electron-microscopic studies have revealed the different stages of film growth. Pashley, et al. [24] have identified the four basic stages of the growth process, namely, nucleation and island structure, coalescence of islands,

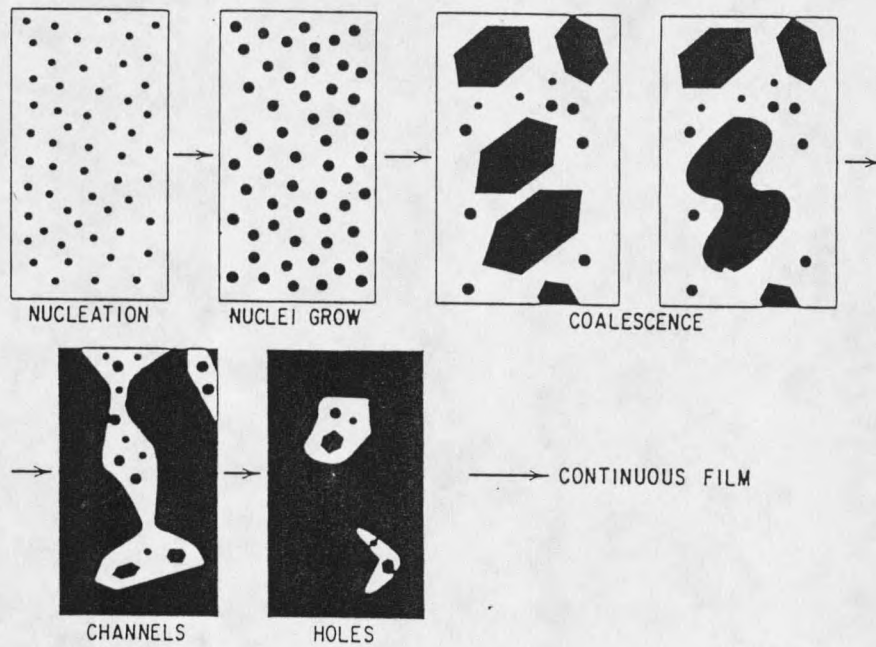
channel formation, and the formation of the continuous film. These stages are shown in Figure 2a and 2b and explained in the following sections [14].

**(1) The Island Stage:** Upon the onset of condensation, the initial nuclei are fairly uniform in size. Although the growth is three-dimensional in nature, the growth parallel to the substrate is greater than that normal to it. This implies growth as a result of surface diffusion of adatoms rather than growth by direct impingement.

**(2) The Coalescence Stage:** As two neighbor nuclei grow, at some point they touch each other and a liquid-like coalescence occurs as shown in Figure 2b. The driving force for coalescence is the reduction of surface energy by the formation of a new composite island which has a smaller surface-to-volume ratio.

A triangular, straight edged shape of the crystallites is characteristic of the late nucleation stage (Figure 2a). During coalescence, these well-defined crystallographic shapes become rounded. Mass transfer may occur by both volume and surface diffusion, but surface diffusion is shown to be the predominant mode. Curvature differences on the surface of the coalescing islands create surface tension forces, which drive atoms on the surface from convex-shaped regions to concave-shaped regions. These forces

(a)



(b)

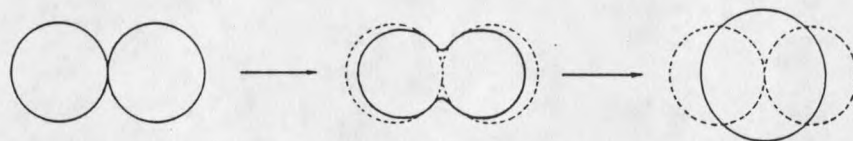


Figure 2. (a) Schematic of the stages of film growth. (b) Schematic of the shape changes during coalescence [24].

are minimized at the end by the formation of a rounded island. As a result, a reduction in area and an increase in height occur which, in turn, reduce the total substrate area covered by the islands.

In addition to surface area reduction, the surface energy is also reduced by rearranging the crystal orientation. After coalescence, preferred boundary planes are observed and the composite island assumes a hexagonal shape.

(3) The Channel Stage: During each coalescence, the smaller nuclei are pulled into more massive regions of the film leaving fresh substrate area for further secondary nucleation. As the islands grow and coalescence takes place continually, the islands become elongated and form larger islands separated by long channels or holes. The channels contain many secondary nuclei, which coalesce with each other and with the main film, thus increasing the main film mass and leaving fresh substrate areas behind for further secondary nucleation. Each repetition of this process makes the channel smaller and the cycle continues until the channel is filled in.

(4) The Continuous Film: Pashley et al. [24] observed that during film growth, especially in the coalescence stage, island orientation changes by recrystallization. A considerable degree of recrystallization occurs even at room

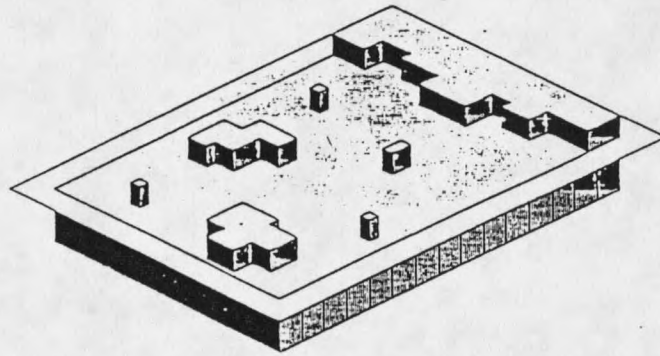
temperature. Each grain in a polycrystalline film incorporates a very large number of initial nuclei. Thus, the resulting number of crystals in a continuous film is significantly less than the initial number of nuclei.

### Growth Modes

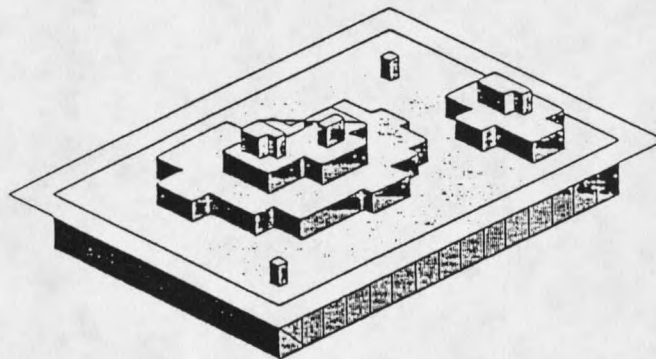
Three basic growth modes are recognized and named after the authors who established them: the Frank-van der Merwe (FM), the Stranski-Krastanov (SK), and Volmer-Weber (VW) modes [25]. These modes are illustrated in Figure 3. Bauer [26,27] has demonstrated that relative surface energies dictate the growth mode. Neglecting edge energies and the shape and size dependence of the surface energies, the equation governing the growth mode is

$$\Delta = \sigma_f + \sigma_i - \sigma_s \quad (3)$$

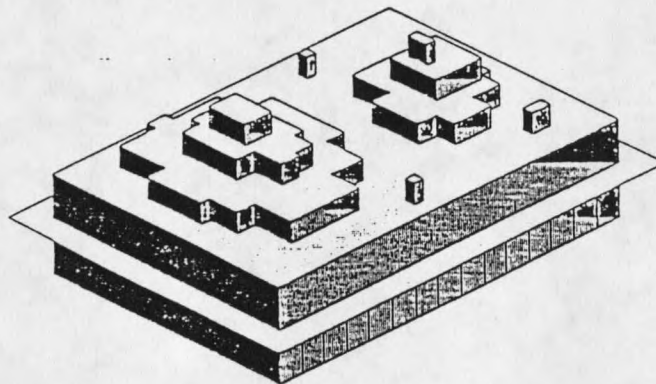
where,  $\sigma_f$  and  $\sigma_s$  are the specific free surface energies of film and substrate, respectively, and  $\sigma_i$  is the specific free interfacial energy. If the deposited material has a higher surface energy than the substrate ( $\Delta > 0$ ), the film will tend to form a three-dimensional structure (VW mode), otherwise a layer by layer growth (FM mode) is favored ( $\Delta \leq 0$ ). When  $\sigma_i$  changes with the size and shape of the island as the layers grow, transitions between the two modes occur and 3-D crystals grow on top of one or a few monolayers (SK mode).



(a)



(b)



(c)

Figure 3. Various modes of growth of an overlayer on a substrate: (a) Frank-van der Merwe, (b) Volmer-Weber, and (c) Stranski-Krastanov growth. The horizontal plane indicates where the substrate ends [25].

### Epitaxial Growth

Epitaxy: from the Greek,  $\epsilon\pi\iota$  (epi: placed or resting upon) +  $\tau\alpha\xi\iota\zeta$  (taxis: arrangement). Epitaxy = "the growth of crystals on a crystalline substrate that determines their orientation" [25].

Frankenheim [28] pioneered the science of epitaxy by demonstrating that sodium nitrate can be grown from a solution onto a calcite crystal with a unique orientation relationship. Royer [29] used x-ray diffraction (XRD) to show that such oriented growth requires that lattice planes in both materials have similar structure and orientation to the substrate material; he concluded that epitaxial growth requires a lattice misfit of not more than about 15%. Lattice misfit,  $\epsilon$ , is defined by

$$\epsilon = \frac{b - a}{a} \quad (4)$$

where,  $a$  and  $b$  are the in-plane lattice constants of substrate and overgrowth, respectively. Thus the occurrence of epitaxial growth is probable whenever the substrate and overgrowth have coincident lattices and low interfacial energy. Lattice mismatch causes a strain at the substrate-overgrowth interface. This strain is relieved by creating misfit dislocations in the overgrowth at the interface. Studies have been carried out to identify and characterize misfit dislocations at epitaxial interfaces [27,30].

## Thin Film Analysis Techniques

### X-ray Diffraction

As a crystallographic analysis method, x-ray diffraction is used for determining substrate orientation, for characterizing crystalline phases and preferred orientations in crystalline layers, and for identifying amorphous regions [31].

X-ray diffraction utilizes the following geometrical arrangements as illustrated in Figure 4:

- (1) The incident beam, the normal to the reflecting plane, and the diffracted beam are always on the same plane.
- (2) The angle between the diffracted beam and the transmitted beam is  $2\theta$ .

Diffraction occurs when the wavelength of the incident beam matches with the repeat distance between scattering centers to form a constructive interference. The criterion to be met for the Bragg law is

$$n\lambda = 2d\sin\theta \quad (5)$$

where,  $\lambda$  is the x-ray wavelength,  $d$  is the interplanar spacing,  $\theta$  is the Bragg diffraction angle, and  $n$  is an integer giving the order of the diffraction. This geometry is illustrated in Figure 4. The experimentally measured angle is usually the diffraction angle,  $2\theta$ , rather than  $\theta$ .







































































































































































































































































































































































































































